

Excellence in Chemistry Research

Announcing our new flagship journal

- Gold Open Access
- Publishing charges waived
- Preprints welcome
- Edited by active scientists



Meet the Editors of *ChemistryEurope*



Luisa De Cola

Università degli Studi
di Milano Statale, Italy



Ive Hermans

University of
Wisconsin-Madison, USA



Ken Tanaka

Tokyo Institute of
Technology, Japan

Antioxidant Activities of Hydroxylated Naphthalenes: The Role of Aryloxy Radicals

Valeria Lino,^[a, b] Paola Manini,^{*[b]} Marco Galeotti,^[c] Michela Salamone,^[c] Massimo Bietti,^[c] Orlando Crescenzi,^[b] Alessandra Napolitano,^[b] and Marco d'Ischia^[b]

Dedicated to Prof. Cesare Gennari on the occasion of his 70th birthday.

Herein is delineated a first systematic framework for the definition of structure-antioxidant property relationships in the dihydroxynaphthalene (DHN) series. The results obtained by a combined experimental and theoretical approach revealed that 1,8-DHN is the best performing antioxidant platform, with its unique hydrogen-bonded *peri*-hydroxylation pattern contributing to a fast H atom transfer process. Moreover, the comparative analysis of the antioxidant properties of DHNs carried out by performing DPPH and FRAP assays and laser flash photolysis experiments, revealed the higher antioxidant power

associated with an α -substitution pattern (i.e. in 1,8- and 1,6-DHN) with respect to DHNs exhibiting a β -substitution pattern (i.e. in 2,6- and 2,7-DHN). DFT calculations and isolation and characterization of the main oligomer intermediates formed during the oxidative polymerization of DHNs supported this evidence by providing unprecedented insight into the generation and fate of the intermediate naphthoxy radicals, which emerged as the main factor governing the antioxidant activity of DHNs.

Introduction

The quest for efficient, sustainable and biocompatible antioxidant systems pervades a variety of research fields, from nanomedicine to food chemistry and industry, packaging and materials science.^[1] Most of the interest in this connection is being devoted to harnessing natural structural motifs endowed with superior hydrogen atom donor and/or electron transfer properties.^[2,3] This trend is exemplified by the growing number of studies on 1,8-dihydroxynaphthalene (1,8-DHN)^[4-9] and polymeric materials thereof. 1,8-DHN is a naturally occurring polyketide derivative involved in the biosynthesis of black allomelanin pigments in various fungi,^[10,11] such as *Aspergillus fumigatus* and *Cladosporium sphaerospermum*. 1,8-DHN-derived allomelanins have been implicated in a variety of biological

activities, from virulence to stress resistance^[12,13] and, especially, protection against harmful ionizing radiation,^[14,15] allowing for example survival of pigmented fungi near the damaged nuclear reactor at Chernobyl.^[16]

The outstanding antioxidant properties of 1,8-DHN include a potent hydrogen atom transfer (HAT) ability in standard assays, e.g. in 2,2-di(4-octylphenyl)-1-picrylhydrazyl radical and the azobisisobutyronitrile-initiated styrene autoxidation assays.^[17] Mechanistic experiments suggested that the potent antioxidant behavior of 1,8-DHN is due to the exceptional stabilization of aryloxy radicals resulting from HAT provided by both intramolecular hydrogen bonding and delocalization over the naphthalene ring system.^[18] Consistent with this conclusion, 1,8-DHN allomelanin was found to exhibit an unusually intense EPR signal and a potent antioxidant ability in the 2,2-diphenyl-1-picrylhydrazyl (DPPH) and ferric reducing antioxidant power (FRAP) assays.^[6]

In the past few years, concomitant with the exploitation of 1,8-DHN allomelanin for a variety of applications,^[9,5,19] the structural architecture of this polymer has been the focus of investigation by chemical and spectroscopic studies, and the main oligomer intermediates in the oxidative polymerization pathway have been isolated and characterized (Figure 1).^[7]

Compared to the other melanin polymers found in nature, such as the nitrogenous eumelanins^[20] produced in mammals by the oxidative polymerization of tyrosine via 5,6-dihydroxyindole (DHI) intermediates, allomelanins from 1,8-DHN were found to exhibit a remarkable stability to oxidation, a property that can be ascribed to the superior antioxidant power of these polymers.^[9] Little is known, however, as to whether the 1,8-dioxygenation pattern is optimally suited to counteract the noxious effects of free radicals and reactive oxygen species, or if there are alternative hydroxylation patterns that may warrant higher antioxidant power and protective performances for

[a] Dr. V. Lino
Scuola Normale Superiore
Piazza dei Cavalieri 7
56126 Pisa (Italy)

[b] Dr. V. Lino, Prof. P. Manini, Prof. O. Crescenzi, Prof. A. Napolitano, Prof. M. d'Ischia
Department of Chemical Sciences
University of Naples Federico II
Via Cintia 4
80126 Napoli (Italy)
E-mail: pmanini@unina.it

[c] M. Galeotti, M. Salamone, M. Bietti
Dipartimento di Scienze e Tecnologie Chimiche
University of Rome "Tor Vergata"
Via della Ricerca Scientifica 1
00133 Rome (Italy)

Supporting information for this article is available on the WWW under <https://doi.org/10.1002/cplu.202200449>

© 2023 The Authors. ChemPlusChem published by Wiley-VCH GmbH. This is an open access article under the terms of the Creative Commons Attribution License, which permits use, distribution and reproduction in any medium, provided the original work is properly cited.

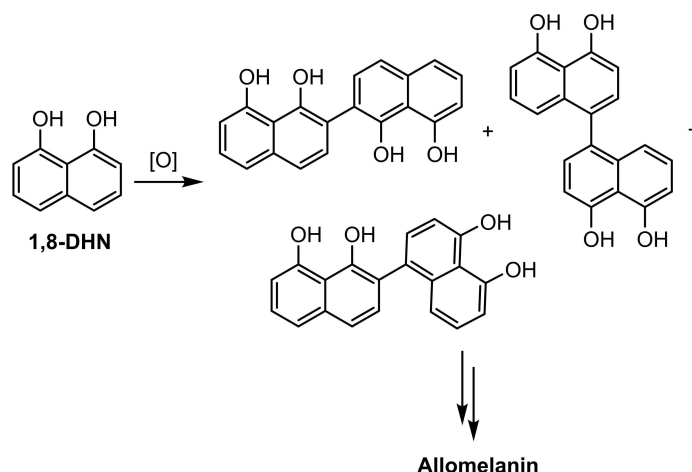


Figure 1. First stages of the oxidative polymerization of 1,8-dihydroxynaphthalene (1,8-DHN).

biomedical and technological applications. To fill this gap, we report herein, to the best of our knowledge, the first comparative investigation of the antioxidant properties and underlying free radical chemistry of a series of isomeric DHN derivatives. This study may be helpful to set the basis for a novel framework of structure-property relationships allowing for the identification of the best performing antioxidant DHN ring systems, and providing the key for the design of novel advanced antioxidants.

Results and Discussion

Substrate selection and rationale of the study. Besides the naturally occurring 1,8-DHN, taken as reference, three isomeric DHN derivatives were selected for this comparative study, 1,6-dihydroxynaphthalene (1,6-DHN) featuring a non-symmetric *meta*-like mixed α/β -substitution pattern, 2,6-dihydroxynaphthalene (2,6-DHN) featuring a β -type *para*-like substitution pattern and 2,7-dihydroxynaphthalene (2,7-DHN) with a symmetric *meta*-like β -substitution pattern. In addition, 1-naphthol (1-HN) and 2-naphthol (2-HN) were included to probe the positional dependence of the antioxidant activity of the α - versus β -OH substituents (Figure 2).

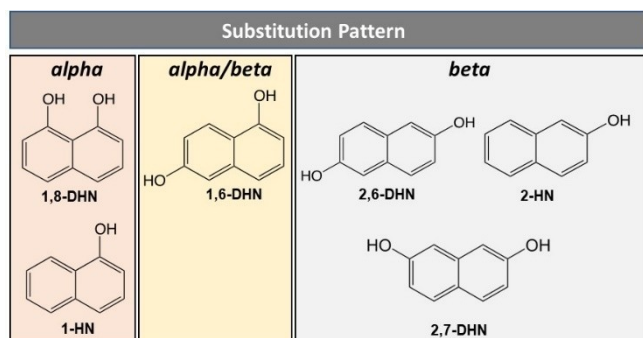


Figure 2. (Di)hydroxynaphthalenes selected for this study.

In all DHNs examined the hydroxyl groups were located on both rings, and isomers producing localized or delocalized quinone moieties were ruled out, with the sole exception of 2,6-DHN for which the hydroxyl substitution pattern is compatible with the formation of a naphthoquinone (NQ)-type product. The rationale was to address how and to what extent the reactivity of different aryloxy radicals can influence the antioxidant activity of these substrates. To this aim, three different experimental approaches were pursued based on the comparative investigation of: a) the antioxidant activity by use of the DPPH and FRAP assays; b) the first stages of the oxidation reaction by means of laser flash photolysis studies on HAT to the cumyloxy radical ($\text{PhC}(\text{CH}_3)_2\text{O}^\bullet$, CumO^\bullet); c) the oxidative polymerization processes through isolation of the oligomeric intermediates.

Antioxidant activity assays. The antioxidant activity of the isomeric DHNs was investigated in comparison with that of 1,8-DHN against reference standards in two different systems: the blue DPPH radical/hydrazine conversion and ferric reducing/antioxidant power (FRAP) assays. These two systems were selected as representative of two different mechanisms of action by which the antioxidant reactivity is actuated, one mediated by HAT (DPPH) and another one by electron transfer (FRAP).

The analysis of the early stages of the DPPH radical decay by monitoring its absorption at 515 nm (Figure 3) showed that 1,8-DHN, 1,6-DHN and 2,6-DHN were more efficient than Trolox, commonly taken as the reference system for this assay; moreover, 1-HN exhibited a reactivity comparable to Trolox whereas 2-HN and 2,7-DHN proved less efficient.

The relatively high antioxidant activity displayed by 1,8-DHN, 1,6-DHN, 2,6-DHN and 1-HN is also supported by data analysis displayed in Table 1. While 1-HN shows a HAT rate constant for the fast step (k_1 value determined after 30 seconds) that is very similar to that obtained for Trolox, k_1 was observed to increase on going to 1,6- and 2,6-DHN, approaching an approximately three-fold increase in the case of 1,8-DHN, for

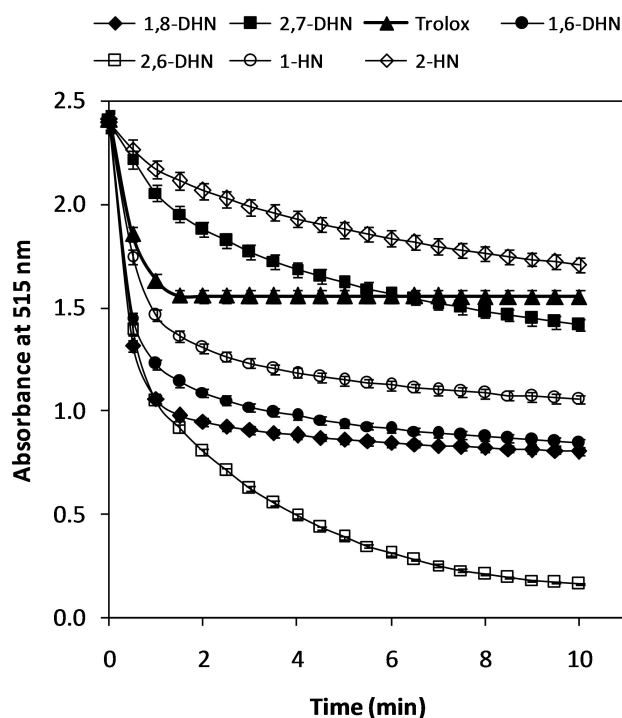


Figure 3. Decrease in absorbance of DPPH (200 μM) monitored at 515 nm in the presence of (di)hydroxynaphthalenes or Trolox (50 μM) in methanol. The mean \pm SD values for three independent experiments are reported.

which the formation of a aryloxy radical highly stabilized by hydrogen bond formation can be envisaged.

Overall, these data suggest that the oxidation pathways involving HAT from α -hydroxyl groups (as for 1-HN and 1,8-DHN) are favoured with respect to those involving β -hydroxyl groups (2-HN and 2,7-DHN).

This hypothesis is also supported by DFT calculations carried out on 1,6-DHN for which both oxidative pathways are accessible. As shown in Table 2, the aryloxy radical from 1,6-DHN formed on the C-1 position (*I*) is energetically more stable, and hence its formation is favoured with respect to the isomeric radical on the C-6 position (*II*).

In this regard, 2,6-DHN represents an exception with a high DPPH consumption that is due to the formation of a stable *p*-quinone intermediate, an event that represents the driving force of the oxidation process.

The relative antioxidant power registered for all the (D)HNs changed slightly when analyzing the process after 10 minutes, with 2,6-DHN affording the highest amount of reduced DPPH. These data correlate well with the stoichiometry (n_{tot}) found for 1,8-DHN, 2,6-DHN, 1,6-DHN and 1-HN (3.0, 3.8, 2.5 and 2.2, respectively), indicating that the reaction can lead to the formation of a pattern of primary oxidation products that are still able to react with DPPH.

Data obtained from the FRAP assay (Table 3) confirmed a higher antioxidant activity for the (D)HNs of the α series, that is 1,8-, 1,6-DHN and 1-HN, with the sole exception of 2,6-DHN for which, as mentioned above, the formation of a stable NQ-type product represents the driving force that accounts for its significantly enhanced reducing power.

Laser flash photolysis experiments. In a subsequent set of experiments the nature of the transient species generated and involved in the antioxidant activity of DHNs and reference HNs was investigated by laser flash photolysis (LFP). Solutions of the compounds in argon-saturated acetonitrile containing 1.0 M dicumyl peroxide (DCMP) were irradiated at 355 nm, at $T = 25^\circ\text{C}$. Under these conditions, the cumyloxy radical is formed and then reacts with the (D)HNs by HAT from the hydroxyl groups (Figure 4).

The kinetic study of the reactions of CumO^\bullet with 1,6-DHN, 2,7-DHN and 2-HN was carried out following the buildup of the naphthoxy radical absorption band at 360 nm (see below) as a function of the concentration of added substrate. In the case of 2,6-DHN, the strong absorption of the substrate at the laser excitation wavelength (355 nm) prevented the spectroscopic study of its reaction with CumO^\bullet .

The time-resolved absorption spectra of the species produced in the reactions of CumO^\bullet with 1,6-, 2,7-DHN and 2-HN are reported in Figure 5.

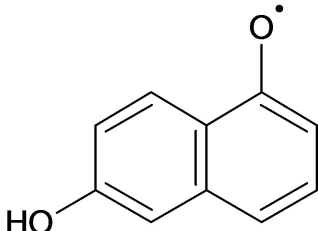
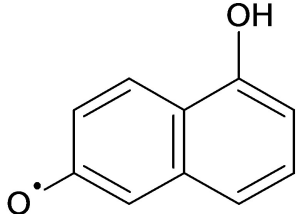
The pertinent second-order rate constants for HAT from the (D)HNs to CumO^\bullet (k_{H}) are collected in Table 4. Also included in this table are the k_{H} values measured previously under analogous experimental conditions for the corresponding reactions of CumO^\bullet with 1,8-DHN and 1-HN.^[18]

In the case of 2-HN (Figure 5a), the decay of CumO^\bullet monitored at 500 nm is accompanied by the buildup of a transient species characterized by two broad absorption bands between 360–410 nm and 440–490 nm, that are assigned to the 2-naphthoxy radical formed following HAT. The decay of these bands occurs with comparable rates, is essentially complete

Table 1. Percentage of reduction, rate constant (k_{r}) and number of H-atoms transferred for the reaction of (di)hydroxynaphthalenes (50 μM) with DPPH (200 μM).^[a]

Compound	DPPH reduced [%] ^[b]	k_{r} [$\text{M}^{-1} \text{s}^{-1}$] ^[c]	n_{tot} ^[d]
1,8-DHN	68.7 \pm 1.8	912 \pm 144	3.0 \pm 0.1
1,6-DHN	62.6 \pm 0.9	419 \pm 88	2.5 \pm 0.2
2,6-DHN	93.6 \pm 0.7	502 \pm 22	3.8 \pm 0.2
2,7-DHN	40.0 \pm 0.3	44 \pm 3	1.7 \pm 0.01
1-HN	53.5 \pm 1.8	311 \pm 71	2.2 \pm 0.2
2-HN	25.8 \pm 1.6	18 \pm 5	1.1 \pm 0.07
Trolox	39.0 \pm 1	328 \pm 37	1.5 \pm 0.2

[a] Values are means \pm SD ($n = 3$). [b] Calculated after 10 min reaction time. [c] Rate constant determined after 30 seconds. [d] Number of H-atoms transferred after 10 min.

Table 2. Stabilities of the aryloxy radicals derived from 1,6-DHN (neutral forms in water) computed at two different theory levels in water (SMD). ^[a]			
Structure	Symmetry	$G_{\text{SMD,RRHO,M06-2X}}^{\text{Ha}^{[b]}}$	$G_{\text{SMD,RRHO,CCSD(T)}}^{\text{Ha}^{[c]}}$
I 	C_s	-535.55667 (0.0)	-534.68408 (0.0)
	C_s	-535.55653 (0.1)	-534.68371 (0.2)
II 	C_s	-535.54780 (5.6)	-534.67589 (5.1)
	C_s	-535.54985 (4.3)	-534.67704 (4.4)

[a] Gibbs free energies were computed in the rigid rotor/harmonic oscillator approximation and include SMD non-electrostatic contributions. In parentheses, relative values (kcal mol^{-1}) referred to the most stable form (in bold). [b] M06-2X/6-311 + +G(2d,2p), SMD//PBE0/6-31 + G(d,p), PCM level. [c] Composite level including evaluation of the electronic energy at the DLPNO-CCSD(T)/cc-pVTZ//PBE0/6-31 + G(d,p), PCM level and addition of solvation contributions from M06-2X/6-311 + +G(2d,2p)//PBE0/6-31 + G(d,p), PCM calculations in vacuo and in water (SMD): see SI for details.

Table 3. Ferric reducing/antioxidant power (FRAP) assay for the (di)hydroxynaphthalenes.	
Compound	FRAP [Trolox eqs] ^[a]
1,8-DHN	2.83 ± 0.06
1,6-DHN	2.00 ± 0.03
2,6-DHN	5.25 ± 0.03
2,7-DHN	0.89 ± 0.02
1-HN	1.69 ± 0.01
2-HN	0.64 ± 0.01

[a] Values are means \pm SD ($n = 3$).

after 100 μs and is accompanied by a residual absorption below 400 nm (Figure 5b). For comparison, the computed UV-vis spectrum of the 2-naphthoxy radical (see SI) also displays two main bands of comparable intensity, centered at 340 and 415 nm.

A similar behavior is observed in the corresponding reaction of 1,6-DHN (Figure 5c) where the decay of CumO^\bullet is accompanied by the buildup of an intense absorption band between

360–410 nm and by two weaker ones between 420–460 and 470–580 nm, that are assigned to the isomeric naphthoxy radicals formed following HAT. The computed UV-vis spectrum of the α radical (see SI), with significant maxima at 360 and 490 nm, matches rather well the experimental one. The computed spectrum of the β radical is roughly similar in this region; however, based on the computed relative free energies, the concentration of this latter species is predicted to be significantly lower. The decay of these bands occurs with comparable rates and is essentially complete after 200 μs and is accompanied by a residual absorption below 400 nm (Figure 5d). A more complex picture is observed in the reaction of 2,7-DHN (Figure 5e), where the decay of CumO^\bullet monitored at 520 nm is accompanied by the buildup of an intense absorption band centered at 360 nm and, on a shorter timescale, of a weaker and very broad one between 390 and 560 nm. The former band shows no significant decay up to 300 μs , whereas the decay of the latter one is essentially complete after 200 μs (Figure 5f). The time-evolution of the spectra results in a

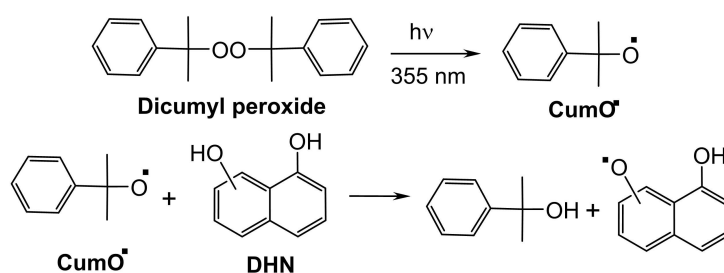


Figure 4. Generation of the cumyloxy radical by LFP and follow-up reaction with dihydroxynaphthalenes.

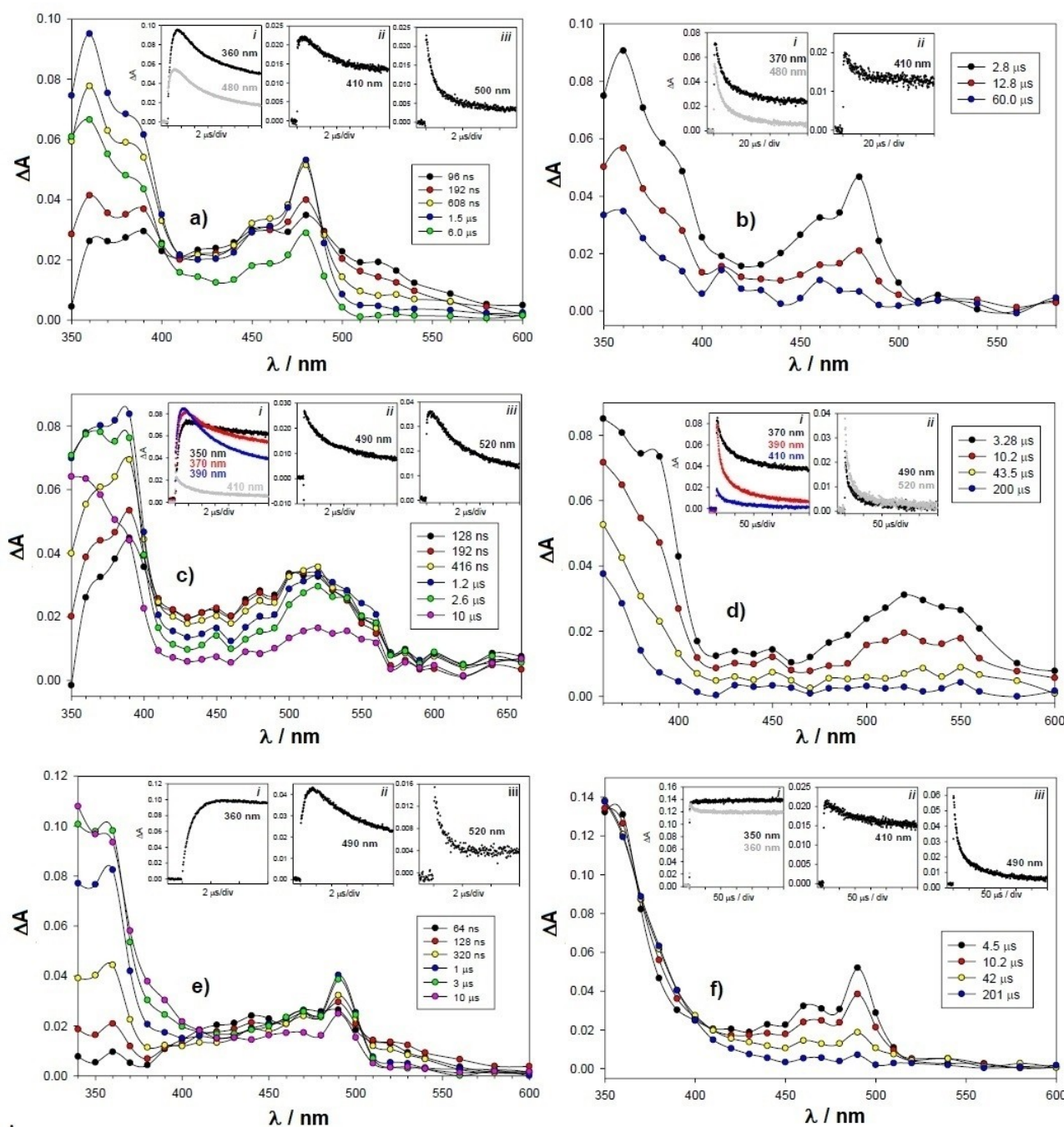


Figure 5. Time-resolved absorption spectra observed after 355 nm LFP of Ar-saturated MeCN solutions ($T = 25^\circ\text{C}$) containing dicumyl peroxide (1.0 M) and: a) 2-HN (19.3 mM) at 96 (black), 192 ns (red), 608 ns (yellow), 1.5 μs (blue), 6.0 μs (green) after the laser pulse. Insets: (i) buildup and consequent decay at 360 and 480 nm; (ii) buildup and consequent decay at 410 nm; (iii) decay at 500 nm. b) 2-HN (19.3 mM) recorded at 2.8 μs (black), 12.8 μs (red) and 60.0 μs (blue) after the laser pulse. Insets: (i) decay at 370 and 480 nm; (ii) buildup and consequent decay at 410 nm. c) 1,6-DHN (4.29 mM) recorded at 128 ns (black), 192 ns (red), 416 ns (yellow), 1.2 μs (blue), 2.6 μs (green), 10 μs (pink) after the laser pulse. Insets: (i) buildup and consequent decay at 350, 370, 390 and 410 nm; (ii) decay at 490 nm; (iii) buildup and consequent decay at 520 nm; d) 1,6-DHN (4.29 mM) recorded at 3.28 μs (black), 10.2 μs (red), 43.5 μs (yellow) and 200 μs (blue) after the laser pulse. Insets: (i) decay at 370, 390 and 410 nm; (ii) decay at 490 and 520 nm. e) 2,7-DHN (7.19 mM) recorded at 64 ns (black), 128 ns (red), 320 ns (yellow), 1.0 μs (blue), 3.0 μs (green), 10 μs (pink) after the laser pulse. Insets: (i) buildup at 360 nm; (ii) buildup and consequent decay at 490 nm; (iii) decay at 520 nm. f) 2,7-DHN (7.19 mM) recorded at 4.5 μs (black), 10.2 μs (red), 42 μs (yellow) and 201 μs (blue) after the laser pulse. Insets: (i) buildup at 350 and 360 nm; (ii) buildup and consequent decay at 410 nm; (iii) decay at 490 nm.

residual absorption below 450 nm. The spectrum computed for the naphthoxyl radicals displays bands at 325 nm and 425 nm, in rather good agreement with the experimental spectrum of the first-formed transient species.

Very interestingly, the spectroscopic features of the residual absorptions observed in the spectra of all three substrates are very similar to that observed previously at long time delays in the reaction of CumO^\bullet with 1,8-DHN, where a stable absorption

Table 4. Second-order rate constants (k_H) for the reactions of CumO* with the (di)hydroxynaphthalenes.^[a]

Substrate	λ_{monit} [nm]	k_H ^[b] [$M^{-1} s^{-1}$]
1,8-DHN ^[c]	360	$3.90 \pm 0.02 \times 10^8$
1,6-DHN	360	$3.60 \pm 0.20 \times 10^8$
1-HN ^[d]	400	$1.43 \pm 0.02 \times 10^8$
2,7-DHN	360	$1.16 \pm 0.06 \times 10^8$
2-HN	360	$5.30 \pm 0.60 \times 10^7$

[a] 355 nm LFP, T = 25 °C, Ar, DCMP 1.0 M; [b] Measured following the buildup of the naphthoxyl radical absorption bands at 360 nm.

band centered at 370 nm was observed and tentatively assigned to the formation of coupling product(s) deriving from dimerization of the intermediate 1,8-DHN naphthoxyl radicals. A similar explanation can be put forward to account for the residual absorption bands observed in the reactions of CumO* with 2-HN, 1,6-DHN and 2,7-DHN.

The k_H values displayed in Table 4 decrease by a factor ~ 7 going from 1,8-DHN to 2-HN. Most interestingly, the decrease in k_H follows the order 1,8-DHN > 1,6-DHN > 1-HN > 2,7-DHN > 2-HN, and parallels those observed in the DPPH (in terms of the n_{tot} parameter) and FRAP assays.

Oligomer isolation and characterization. In a final series of experiments, to further address the influence of the hydroxyl groups and of their relative position on the oxidative susceptibility of the naphthalene ring, the mechanism of polymerization of the DHNs was investigated by the structural characterization of the main isolable oligomeric intermediates. To this aim, a previously reported standard protocol was adopted, involving the oxidation of the substrate by the horseradish peroxidase (HRP)/H₂O₂ system in 0.1 M phosphate buffer at pH 7.0.^[4,7] The oligomer intermediates were isolated as the acetyl derivatives and their structures were determined by 1D/2D NMR spectroscopy and mass spectrometry (Figure 6).

A comparative inspection of the structures together with those of the previously isolated dimers from 1,8-DHN^[7] revealed a prevalent tendency to couple via C–C connections between the dihydroxynaphthalene units in *ortho* to the naphthoxyl group, even when the alternate *para* mode is accessible. This finding confirms previous data on 1,8-DHN, for which DFT calculations predicted more favorable 2,2'-coupling over 4,4'-coupling^[18] (see SI). In good agreement with the data obtained from the antioxidant assays and LFP experiments, the oxidation process proceeds through the formation of naphthoxyl radicals which undergo predominant C–C couplings at the C-2 position, in the case of an α substitution pattern (i.e. in 1-HN and 1,8-DHN), and at the C-1 position, in the case of a β substitution pattern (i.e. in 2,6-DHN, 2,7-DHN and 2-HN).

As expected, a borderline reactivity emerged from the analysis of the structures of the dimers isolated from 1,6-DHN as a consequence of the presence of both α and β hydroxyl groups (Figure 7). In this case, the preferential formation of the α naphthoxyl radical (*I*) first and then of the 2,2'-dimer 1, may be explained considering the higher stability of *I*, as evidenced by the results of DFT calculations (see Table 2). The influence of the α substitution pattern on the susceptibility of the

naphthalene ring to oxidation is still evident in the dimer 1 for which the formation of naphthoxyl radical *III* is favoured (see SI).

Conclusion

The results of the integrated approach to the antioxidant activity of isomeric DHNs reported in this study have disclosed some structure-dependent facets of the reactivity of the (D)HN platform:

- 1) substrates bearing α -hydroxyl groups exhibit an enhanced electron transfer and HAT reactivity compared to those bearing β -hydroxyl groups, as shown by the results of the antioxidant activity assays and LFP studies;
- 2) access to extended-quinone species provides a most favorable channel for electron transfer via evolution of the semiquinone-like naphthoxyl radical, but not for chain breaking effects;
- 3) ortho-ortho coupling patterns dominate the structures of the main oligomer intermediates, enabling in the favorable cases the generation of BINOL-type substructures which are especially prone to further reactive pathways.

Overall, these results: a) confirmed and supported the highest antioxidant power of 1,8-DHN due to the unique hydrogen-bonded *peri*-hydroxylation pattern contributing to the high stabilization of the corresponding naphthoxyl radical; b) pointed out for the first time the enhanced antioxidant activity associated with the α -hydroxynaphthalene ring system (e.g. 1,8-DHN, 1,6-DHN and 1-HN).

Besides the well-established high potential of the 1,8-DHN platform, the antioxidant power exhibited by 1,6-DHN and 1-HN proved to be remarkable enough, especially when compared to Trolox, widely recognized as a powerful antioxidant. This evidence opens to multiple opportunities for the design of next generation antioxidants based on the α -hydroxynaphthalene ring system, beyond the traditional catechol-pyrogallol paradigm that currently dominates the field.

Experimental Section

Antioxidant assays

DPPH. A 200 μM DPPH solution in methanol (1.98 mL) was added under stirring to a 5 mM solution of the selected (D)HN in methanol (20 μL). The reaction was monitored by UV-vis analysis by measuring the absorbance at 515 nm every 30s for 10 min. Trolox was used as the reference compound. Experiments were run in triplicate. The percentage of reduction, rate constant (k_r) and number of H-atoms transferred for the reaction (n_{tot}) are calculated according to the literature.^[21]

FRAP. The FRAP reagent was prepared freshly by mixing 0.3 M acetate buffer (pH 3.6), 10 mM 2,4,6-tris(2-pyridyl)-s-triazine in 40 mM HCl, and 20 mM ferric chloride in water, in the ratio 10:1:1.^[22] The FRAP reagent was added to a 1 mg/mL methanol solution of the selected (D)HN (2–15 μL). The mixture was taken under vigorous stirring at room temperature and after 10 min the absorbance at 593 nm was measured. Trolox was used as the

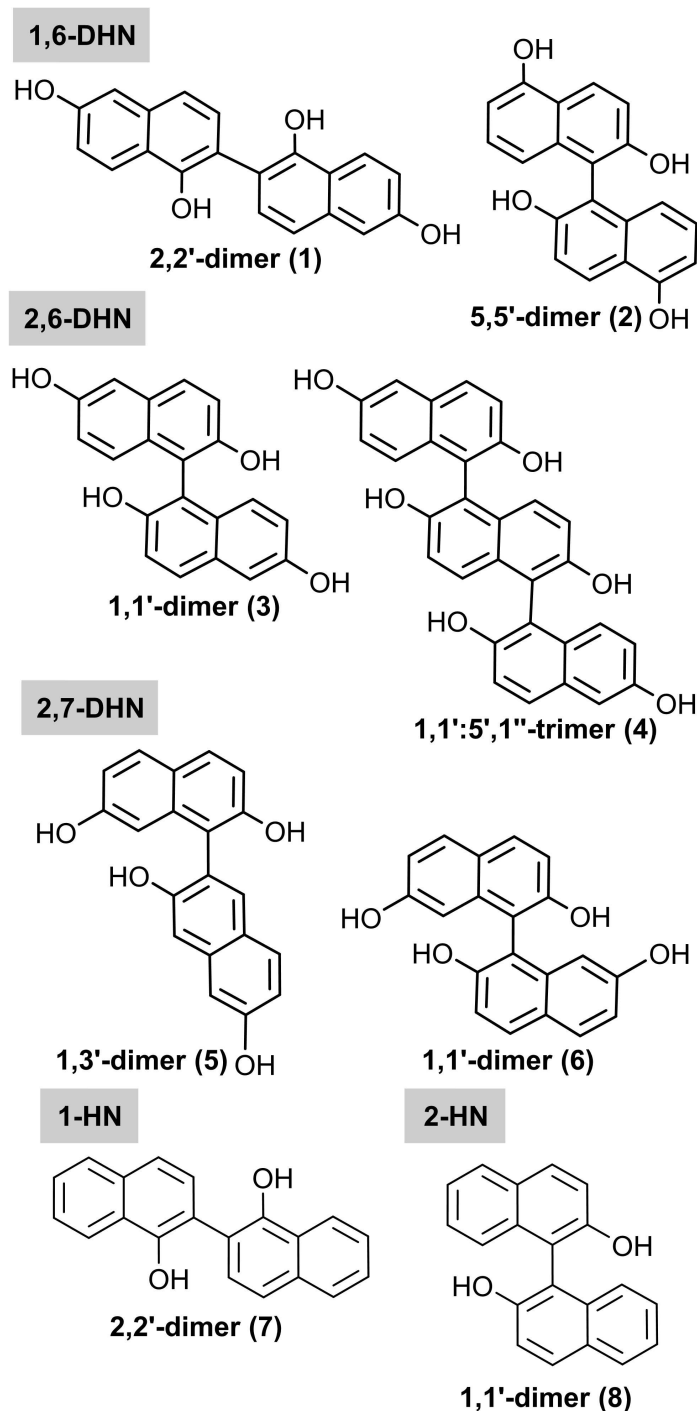


Figure 6. Oligomeric intermediates isolated as acetyl derivatives from the oxidation reaction of 1,6-DHN, 2,6-DHN, 2,7-DHN, 1-HN and 2-HN.

reference compound and the results were expressed as Trolox equivalents. Experiments were run in triplicate.

Synthesis of oligomeric intermediates: general procedure. A 20 mM solution of the proper (D)HN in aqueous phosphate buffer (0.1 M, pH 7) was treated under vigorous stirring with horseradish peroxidase (HRP, 15 U/mL) and H_2O_2 (1.2 eqs).^[4,7] After the proper reaction time (1,8-DHN 5 s, 2,6-DHN 45 s, 2,7-DHN 45 s, 1,6-DHN 16 s, 1-HN and 2-HN 5 min), the mixture was treated with sodium dithionite and extracted with water/ethyl acetate. The organic fractions were dried on anhydrous sodium sulphate and evaporated

under reduced pressure. The residue was treated with acetic anhydride and pyridine overnight. The acetylated mixture was subjected to liquid chromatography on silica gel to afford the pure oligomers.

Laser flash photolysis experiments. Laser flash photolysis experiments were carried out with an Applied Photophysics LK-60 laser kinetic spectrometer providing 8 ns pulses, using the third harmonic (355 nm) of a Quantel Brilliant-B Q-switched Nd:YAG laser. The laser energy was adjusted to ≤ 10 mJ/pulse by the use of the appropriate filter. A 3.5 mL Suprasil quartz cell (10 mm \times 10 mm) was used for all

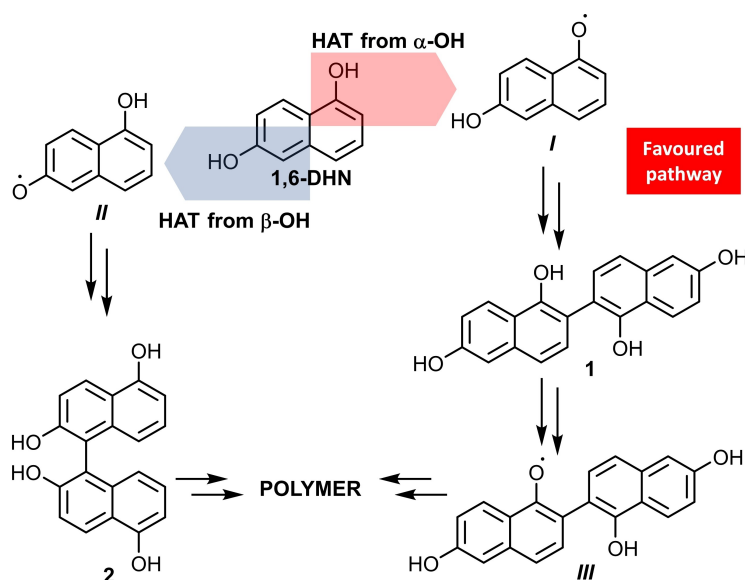


Figure 7. Schematic outline of the first stages in the oxidative polymerization of 1,6-DHN.

the experiments. N_2 -saturated CH_3CN solutions of dicumyl peroxide (1 M) and (D)HNs (1.5–14 mM) were used. All the experiments were carried out at $T = 25 \pm 0.5$ °C under magnetic stirring. Data were collected at individual wavelengths with an Agilent Infinium oscilloscope and analyzed with the kinetic package implemented in the instrument. Observed rate constants (k_{obs}) were obtained by monitoring the change of absorbance at the maximum absorption wavelengths of the product naphthoxyl radicals by averaging 3–5 values. Each trace obeyed a first-order kinetic and second order rate constants (k_{II}) were obtained from the slopes of the plots of k_{obs} vs substrate concentration.

Computational studies. Calculations were mostly performed with the Gaussian package of programs.^[23] DLPNO-CCSD(T) calculations were performed with Orca 4.2.1.^[24,25]

All structures were geometry optimized at the DFT level with the PBE0 functional,^[26] the PBE hybrid including 25% exact exchange, and a reasonably large basis set [6-31+G(d,p)]. The spin-unrestricted formulation was adopted for doublet states. For each species, different oxidation states as well as different tautomers/conformers were explored. Single point energy calculations were also performed with the M06-2X functional^[27] in combination with the large 6-311++G(2d,2p) basis set.

Computations were performed either in vacuo, or by adoption of a polarizable continuum medium (PCM)^[28–31] to account for the influence of the solution environment. In view of the faster convergence, a scaled van der Waals cavity based on universal force field (UFF) radii^[32] was used, and polarization charges were modeled by spherical Gaussian functions,^[33,34] non-electrostatic contributions to the solvation free energy were disregarded at this stage: these terms were accounted for in single-point PCM calculations (at the PCM geometries) employing radii and non-electrostatic terms of the SMD solvation model.^[35] Vibrational-rotational contributions to the free energy (298.15 K, 1 atm) were also computed.

Domain-based local pair natural orbital coupled-cluster (DLPNO-CCSD(T)) calculations^[36,37] were performed with the cc-pVTZ and with a “TightPNO” pair natural orbital setting. For a uniform treatment of open- and closed-shell species, the “Use-FullLMP2Guess” keyword was set to “false” for the closed shell calculations.

UV-vis spectra of the main species were computed in vacuo or in solution using the time-dependent density functional theory (TD-DFT) approach,^[38–42] with the PBE0 functional and the 6-311++G(2d,2p) basis set. To produce graphs, transitions below 5.6 eV were selected, and an arbitrary Gaussian line width of 0.25 eV was imposed; the spectra were finally converted to a wavelength scale.

Acknowledgements

This study has been carried out in the frame of the project SAPIENT (2017CBHCWF) funded by MIUR (PRIN-2017). Open Access funding provided by Università degli Studi di Napoli Federico II within the CRUI-CARE Agreement.

Conflict of Interest

The authors declare no conflict of interest.

Data Availability Statement

The data that support the findings of this study are available in the supplementary material of this article.

Keywords: antioxidants · dihydroxynaphthalenes · electron transfer · hydrogen atom transfer · laser flash photolysis · radicals

[1] C. Pedro, O. G. Paniz, I. A. A. Fernandes, D. G. Bortolini, F. T. V. Rubio, C. W. I. Haminiuk, G. M. Maciel, W. L. E. Magalhães, *Antioxidants* **2022**, *11*, 1644.

[2] M. Reali, A. Gouda, J. Bellemare, D. Ménard, J.-M. Nunzi, F. Soavi, C. Santato, *ACS Appl. Bio Mater.* **2020**, *3*, 5244–5252.

- [3] M. Sheliakina, A. B. Mostert, P. Meredith, *Adv. Funct. Mater.* **2018**, *28*, 1805514.
- [4] V. Lino, P. Manini, *ACS Omega* **2022**, *7*, 15308–15314.
- [5] N. C. McCallum, F. A. Son, T. D. Clemons, S. J. Weigand, K. Gnanasekaran, C. Battistella, B. E. Barnes, H. Abeyratne-Perera, Z. E. Siwicka, C. J. Forman, X. Zhou, M. H. Moore, D. A. Savin, S. I. Stupp, Z. Wang, G. J. Vora, B. J. Johnson, O. K. Farha, N. C. Gianneschi, *J. Am. Chem. Soc.* **2021**, *143*, 4005–4016.
- [6] P. Manini, V. Lino, P. Franchi, G. Gentile, T. Sibillano, C. Giannini, E. Picardi, A. Napolitano, L. Valgimigli, C. Chiappe, M. A. d'Ischia, *Chem-PlusChem* **2019**, *84*, 1331–1337.
- [7] M. M. Cecchini, S. Reale, P. Manini, M. d'Ischia, F. De Angelis, *Chem. Eur. J.* **2017**, *23*, 8092–8098.
- [8] P. Manini, V. Lino, G. D'Errico, S. Reale, A. Napolitano, F. De Angelis, M. d'Ischia, *Polym. Chem.* **2020**, *11*, 5005–5010.
- [9] P. Manini, V. Lucci, V. Lino, S. Sartini, F. Rossella, G. Falco, C. Chiappe, M. d'Ischia, *J. Mater. Chem. B* **2020**, *8*, 4412–4418.
- [10] J. D. Nosanchuk, R. E. Stark, A. Casadevall, *Front. Microbiol.* **2015**, *6*, 1463.
- [11] M. J. Butler, A. W. Day, *Can. J. Microbiol.* **1998**, *44*, 1115–1136.
- [12] J. D. Nosanchuk, A. Casadevall, *Cell. Microbiol.* **2003**, *5*, 203–223.
- [13] A. Casadevall, A. L. Rosas, J. D. Nosanchuk, *Curr. Opin. Microbiol.* **2000**, *3*, 354–358.
- [14] C. Pacelli, R. A. Bryan, S. Onofri, L. Selbmann, I. Shuryak, E. Dadachova, *Environ. Microbiol.* **2017**, *19*, 1612–1624.
- [15] C. Pacelli, L. Selbmann, R. Moeller, L. Zucconi, A. Fujimori, S. Onofri, *Front. Microbiol.* **2017**, *8*, 2002.
- [16] A. Casadevall, R. Cordero, R. Bryan, J. Nosanchuk, E. Dadachova, *Microbiol. Spectr.* **2017**, *5*.
- [17] M. C. Foti, E. R. Johnson, M. R. Vinqvist, J. S. Wright, L. R. C. Barclay, K. U. Ingold, *J. Org. Chem.* **2002**, *67*, 5190–5196.
- [18] P. Manini, M. Bietti, M. Galeotti, M. Salamone, O. Lanzalunga, M. M. Cecchini, S. Reale, O. Crescenzi, A. Napolitano, F. De Angelis, V. Barone, M. d'Ischia, *ACS Omega* **2018**, *3*, 3918–3927.
- [19] X. Zhou, N. C. McCallum, Z. Hu, W. Cao, K. Gnanasekaran, Y. Feng, J. F. Stoddart, Z. Wang, N. C. Gianneschi, *ACS Nano* **2019**, *13*, 10980–10990.
- [20] F. Solano, *New J. Sci.* **2014**, *2014*, 498276.
- [21] P. Goupy, C. Dufour, M. Loonis, O. Dangles, *J. Agric. Food Chem.* **2003**, *51* (3), 615–622.
- [22] I. F. F. Benzie, J. J. Strain, *Anal. Biochem.* **1996**, *239*, 70–76.
- [23] M. J. Frisch, G. W. Trucks, H. B. Schlegel, G. E. Scuseria, M. A. Robb, J. R. Cheeseman, G. Scalmani, V. Barone, B. Mennucci, G. A. Petersson, H. Nakatsuji, M. Caricato, X. Li, H. P. Hratchian, A. F. Izmaylov, J. Bloino, G. Zheng, J. L. Sonnenberg, M. Hada, M. Ehara, K. Toyota, R. Fukuda, J. Hasegawa, M. Ishida, T. Nakajima, Y. Honda, O. Kitao, H. Nakai, T. Vreven, J. A. Montgomery, Jr., J. E. Peralta, F. Ogliaro, M. Bearpark, J. J. Heyd, E. Brothers, K. N. Kudin, V. N. Staroverov, T. Keith, R. Kobayashi, J. Normand, K. Raghavachari, A. Rendell, J. C. Burant, S. S. Iyengar, J. Tomasi, M. Cossi, N. Rega, J. M. Millam, M. Klene, J. E. Knox, J. B. Cross, V. Bakken, C. Adamo, J. Jaramillo, R. Gomperts, R. E. Stratmann, O. Yazyev, A. J. Austin, R. Cammi, C. Pomelli, J. W. Ochterski, R. L. Martin, K. Morokuma, V. G. Zakrzewski, G. A. Voth, P. Salvador, J. J. Dannenberg, S. Dapprich, A. D. Daniels, O. Farkas, J. B. Foresman, J. V. Ortiz, J. Cioslowski, D. J. Fox, Gaussian 09, Revision D.01; Gaussian, Inc., Wallingford CT, **2013**.
- [24] F. Neese, *Wiley Interdiscip. Rev.: Comput. Mol. Sci.* **2012**, *2*, 73–78.
- [25] F. Neese, *Wiley Interdiscip. Rev.: Comput. Mol. Sci.* **2017**, *8*, e1327.
- [26] C. Adamo, V. Barone, *J. Chem. Phys.* **1999**, *110*, 6158–6169.
- [27] Y. Zhao, D. G. Truhlar, *Theor. Chem. Acc.* **2008**, *120*, 215–241.
- [28] S. Miertus, E. Scrocco, J. Tomasi, *J. Chem. Phys.* **1981**, *55*, 117–129.
- [29] M. Cossi, G. Scalmani, N. Rega, V. Barone, *J. Chem. Phys.* **2002**, *117*, 43–54.
- [30] G. Scalmani, V. Barone, K. N. Kudin, C. S. Pomelli, G. E. Scuseria, M. J. Frisch, *Theor. Chem. Acc.* **2004**, *111*, 90–100.
- [31] J. Tomasi, B. Mennucci, R. Cammi, *Chem. Rev.* **2005**, *105*, 2999–3093.
- [32] A. K. Rappé, C. J. Casewit, K. S. Colwell, W. A. Goddard, III, W. M. Skiff, *J. Am. Chem. Soc.* **1992**, *114*, 10024–10035.
- [33] D. A. York, M. Karplus, *J. Phys. Chem. A* **1999**, *103*, 11060–11079.
- [34] G. Scalmani, M. J. Frisch, *J. Chem. Phys.* **2010**, *132*, 114110.
- [35] A. V. Marenich, C. J. Cramer, D. G. Truhlar, *J. Phys. Chem. B* **2009**, *113*, 6378–6396.
- [36] C. Riplinger, P. Pinski, U. Becker, E. F. Valeev, F. Neese, *J. Chem. Phys.* **2016**, *144*, 024109.
- [37] M. Saitow, U. Becker, C. Riplinger, E. F. Valeev, F. Neese, *J. Chem. Phys.* **2017**, *146*, 164105.
- [38] R. E. Stratmann, G. E. Scuseria, M. J. Frisch, *J. Chem. Phys.* **1998**, *109*, 8218–8224.
- [39] R. Bauernschmitt, R. Ahlrichs, *Chem. Phys. Lett.* **1996**, *256*, 454–464.
- [40] M. E. Casida, C. Jamorski, K. C. Casida, D. R. Salahub, *J. Chem. Phys.* **1998**, *108*, 4439–4449.
- [41] C. Adamo, G. E. Scuseria, V. Barone, *J. Chem. Phys.* **1999**, *111*, 2889–2899.
- [42] G. Scalmani, M. J. Frisch, B. Mennucci, J. Tomasi, R. Cammi, V. Barone, *J. Chem. Phys.* **2006**, *124*, 094107.

Manuscript received: December 13, 2022
Revised manuscript received: January 9, 2023
Accepted manuscript online: January 10, 2023